The Plant Cell, Vol. 18, 350–365, February 2006, www.plantcell.org

Arabidopsis Ribonucleotide Reductases Are Critical for Cell Cycle Progression, DNA Damage Repair, and Plant Development [W][OA]

Chunxin Wang and Zhongchi Liu[1]

Department of Cell Biology and Molecular Genetics, University of Maryland, College Park, Maryland 20742

Ribonucleotide reductase (RNR), comprising two large (R1) and two small (R2) subunits, catalyzes a rate-limiting step in the production of deoxyribonucleotides needed for DNA replication and repair. Previous studies in yeast and mammals indicated that defective RNR often led to cell cycle arrest, growth retardation, and p53-dependent apoptosis, whereas abnormally increased RNR activities led to higher mutation rates. Because plants are constantly exposed to environmental mutagens and plant cells are totipotent, an understanding of RNR function in plants is important. We isolated and characterized mutations in all three *R2* genes (*TSO2*, *RNR2A*, and *RNR2B*) in *Arabidopsis thaliana*. *tso2* mutants had reduced deoxyribonucleoside triphosphate (dNTP) levels and exhibited developmental defects, including callus-like floral organs and fasciated shoot apical meristems. *tso2* single and *tso2 rnr2a* double mutants were more sensitive to UV-C light, and *tso2 rnr2a* seedlings exhibited increased DNA damage, massive programmed cell death, and release of transcriptional gene silencing. Analyses of single and double *r2* mutants demonstrated that a normal dNTP pool and RNR function are critical for the plant response to mutagens and proper plant development. The correlation between DNA damage accumulation and the subsequent occurrence of apoptotic nuclei in *tso2 rnr2a* double mutants suggests that perhaps plants, like animals, can initiate programmed cell death upon sensing DNA damage.

INTRODUCTION

Plants are distinct from animals in their lifestyle and their development. A sedentary lifestyle subjects plants to constant exposure to environmental mutagens, including UV irradiation and reactive oxygen species. Accordingly, plants must have evolved active surveillance mechanisms to protect their genomic integrity. A key element for genome surveillance is DNA repair. This essential function of plants must be tightly regulated by the surveillance mechanisms known as DNA damage checkpoint pathways.

Ribonucleotide reductase (RNR) is an important target of the DNA damage checkpoint pathways in yeast, mammals, and possibly higher plants (Huang et al., 1998). RNR catalyzes the reduction of all four ribonucleotide diphosphates (NDPs) into their corresponding deoxyribonucleosides (dNDPs), a rate-limiting step in DNA precursor synthesis (Elledge et al., 1992; Kolberg et al., 2004). RNR consists of two large subunits (R1) and two small subunits (R2). The R2 subunit houses the di-iron tyrosyl radical cofactor essential for the reduction of NDP to dNDP. The well-known chemotherapeutic agent hydroxyurea is a specific but reversible inhibitor of the R2 subunit, acting as a scavenger of the tyrosyl free radical. The R1 subunit binds the nucleoside diphosphate substrates and allosteric effectors to ensure the production of a balanced deoxyribonucleoside triphosphate (dNTP) pool. R1 is the target of feedback regulation, which ensures that dNTPs are not overproduced and that enough NDPs are left for RNA synthesis.

Genetic analyses of *rnr* mutants in yeast and mammals indicated that defective RNR often led to cell cycle arrest, growth retardation, and p53-dependent apoptosis. For example, failure to maintain a sufficient and balanced dNTP pool can lead to misincorporation of dNTPs into DNA, resulting in genetic abnormalities and cell death, as shown in the murine hemopoietic cell line (Oliver et al., 1996). Defective feedback regulation of R1 in budding yeast led to increased dNTP levels, resulting in increased mutation rates but enhanced resistance to mutagens (Chabes et al., 2003a). Loss-of-function *rnr1* and *rnr2* mutants of budding yeast showed depleted dNTP pools and displayed a *cdc* terminal phenotype, arresting at S/G2-phase as a large budded cell (Elledge et al., 1992). In humans, p53R2, an RNR small subunit, is a direct regulatory target of the tumor-suppressor protein p53 (Tanaka et al., 2000). It was suggested that p53R2 supplies dNDPs to the DNA damage-repair system outside the S-phase of the cell cycle. Most of the p53R2 knockout mice died from severe renal failure by the age of 14 weeks, and a greater number of apoptotic cells in kidneys were detected (Kimura et al., 2003). These genetic studies in mammals and fungi demonstrated that RNR plays a key role in maintaining genomic stability.

[1] To whom correspondence should be addressed. E-mail zliu@umd.edu; fax 301-314-9082.
The author responsible for distribution of materials integral to the findings presented in this article in accordance with the policy described in the Instructions for Authors (www.plantcell.org) is: Zhongchi Liu (zliu@umd.edu).
[W]Online version contains Web-only data.
[OA]Open Access articles can be viewed online without a subscription.
Article, publication date, and citation information can be found at www.plantcell.org/cgi/doi/10.1105/tpc.105.037044.

Considering the critical role of RNR in DNA synthesis and repair, it is not surprising that RNR expression and activity are under exquisite control both transcriptionally and posttranscriptionally, as shown by studies of yeast and mammalian cells. These include controlled degradation of RNR protein by Anaphase-Promoting Complex-Cdh1–mediated proteolysis in mouse (Chabes et al., 2003b), the redistribution of RNR2 and RNR4 proteins from nucleus to cytoplasm in response to DNA damage in yeast (Liu et al., 2003; Yao et al., 2003), the control of RNR mRNA stability by the yeast cytoplasmic Constitutive Invertase Derepression13 poly(A) polymerase (Saitoh et al., 2002), the inhibition of RNR activity by the Suppressor of *mec1* Lethality1 protein in yeast (Chabes et al., 1999; Zhao et al., 2000), and the repression of RNR transcription by Constitutive RNR Transcription1, a yeast homolog of the mammalian RFX family of DNA binding proteins (Huang et al., 1998). The existence of multiple regulatory mechanisms for RNR activities underscores the importance of a proper dNTP pool for the fitness and survival of an organism.

In contrast with yeast and mammals, our knowledge of RNR function and regulation in plants is limited. *R1* and *R2* genes have been isolated from tobacco (*Nicotiana tabacum*) and *Arabidopsis thaliana* (Philipps et al., 1995; Chaboute et al., 1998), and their S-phase–specific expression was shown to depend on the *E2F*-like motifs in their promoters (Chaboute et al., 2000, 2002). Transient translocation of a green fluorescent protein–R1 protein from cytoplasm to nucleus in response to UV irradiation was reported recently (Lincker et al., 2004). However, no mutation in any of the plant *RNR* genes has been reported, and the function of *RNR* in maintaining plant genomic stability and genetic variability has not yet been demonstrated.

Here, we report the functional dissection of *RNR* in higher plants. Mutations in *TSO2* were isolated in ethyl methanesulfonate (EMS) mutagenesis screens that caused defects in shoot apical meristem (SAM), flowers, leaves, and fertility. We show that *TSO2* encodes one of the three *R2* genes in *Arabidopsis*, revealing a direct role of *TSO2* in DNA replication. Subsequent identification and characterization of mutations in all three *R2* genes in the *Arabidopsis* genome provided insights into *RNR* function for plant growth and development and the response to environmental mutagens. More significantly, extensive programmed cell death (PCD) was found in *tso2 rnr2a* double mutants, which correlated with accumulating DNA damage in this double mutant. One possible explanation for this correlation between DNA damage and PCD is that perhaps plants, like animals, can initiate PCD upon DNA damage, despite the absence of a p53 homolog in the *Arabidopsis* genome. Finally, release of transcriptional gene silencing (TGS) was observed in *tso2 rnr2a* double mutants, demonstrating an interesting link between DNA replication/chromosome integrity and epigenetic inheritance.

RESULTS

tso2 Mutants Exhibit Various Developmental Defects

Four independent *tso2* mutants (*tso2-1*, *-2*, *-3*, and *-4*) were isolated from EMS mutagenesis screens in the *Arabidopsis* Landsberg *erecta* (L*er*) background (see Methods). These mutants were named *tso2* because of their resemblance to *tso1* mutants, with *TSO* meaning ''ugly'' in Chinese (Liu et al., 1997). All four *tso2* alleles are recessive and phenotypically similar to each other. Therefore, *tso2-1* was chosen for further analysis. At the seedling stage, *tso2-1* mutants were similar to the wild type, with normal roots, cotyledons, and young leaves. Abnormalities first appeared in the fifth rosette leaf and persisted in all subsequent leaves, floral organs, and siliques. The abnormalities included white sectors in green organs (Figures 1A and 1B), uneven thickness, rough surfaces, and irregular margins of leaves or floral organs (Figures 1C and 1D). Stamens occasionally exhibited carpel characteristics indicating homeotic transformation (Figure 1E). The rough and uneven sepals apparently resulted from abnormally enlarged cells as well as cell clusters projecting above the epidermis (Figures 1F and 1G). The white sectors appeared to result from an absence of chloroplasts in patches of mesophyll cells and the formation of large air spaces or tiny cells in subepidermal cell layers (Figures 1H and 1I). Occasionally, *tso2* mutants exhibited fasciated stems on which a single SAM, a group of self-renewing cells at the shoot tip, was enlarged and split into multiple SAMs (Figures 1J to 1L). Finally, *tso2* mutants exhibited reduced fertility, with ~29% aborted seeds (Figure 1M).

TSO2 Encodes a Small Subunit of RNR

Using a map-based cloning approach, we isolated the *TSO2* gene and showed that *TSO2* encodes the small subunit (R2; At3g27060) of RNR (see Methods). Alignment of R2 proteins from different species revealed 16 amino acids that are absolutely conserved from bacteria and plants to human. These invariant residues are distributed throughout the protein. *tso2-1*, *tso2-2*, *tso2-3*, and *tso2-4* are all caused by missense mutations affecting either invariant or highly conserved amino acids (Figure 2A). *tso2-1* and *tso2-4* affect the same invariant Asp-49 residue known to be involved in binding to the R1 large subunit (Philipps et al., 1995). *tso2-2* and *tso2-3* affect Gly-170 and Arg-97, respectively, which reside in areas important for iron binding and for tyrosyl radical environment (Philipps et al., 1995).

Do the *tso2* mutations cause abnormal dNTP levels? We measured dNTP levels in *tso2-1* mutants using a polymerase-based method (Roy et al., 1999). We found that in wild-type *Arabidopsis*, the relative levels of the four dNTPs with respect to each other were similar to those of other organisms, with dTTP the most abundant and dGTP the least abundant (Figure 2B). *tso2-1* floral tissues were found to contain significantly reduced levels of all four dNTPs (Figure 2B). Although dGTP level was reduced to 60% of the wild-type level, dCTP was reduced to 35% of the wild-type level. These differential reductions in dNTPs could lead to an imbalanced dNTP pool in *tso2-1* floral tissues. Therefore, a reduced and possibly imbalanced dNTP pool may underlie the various phenotypes observed in *tso2-1* mutants.

Functional Redundancy among the Three *RNR* Genes

Because *tso2* mutants are all viable and fertile, redundant genes in the *Arabidopsis* genome may compensate for defective *tso2*. Examination of the *Arabidopsis* genome revealed two additional *R2* genes named *RNR2A* (At3g23580) and *RNR2B* (At5g40942

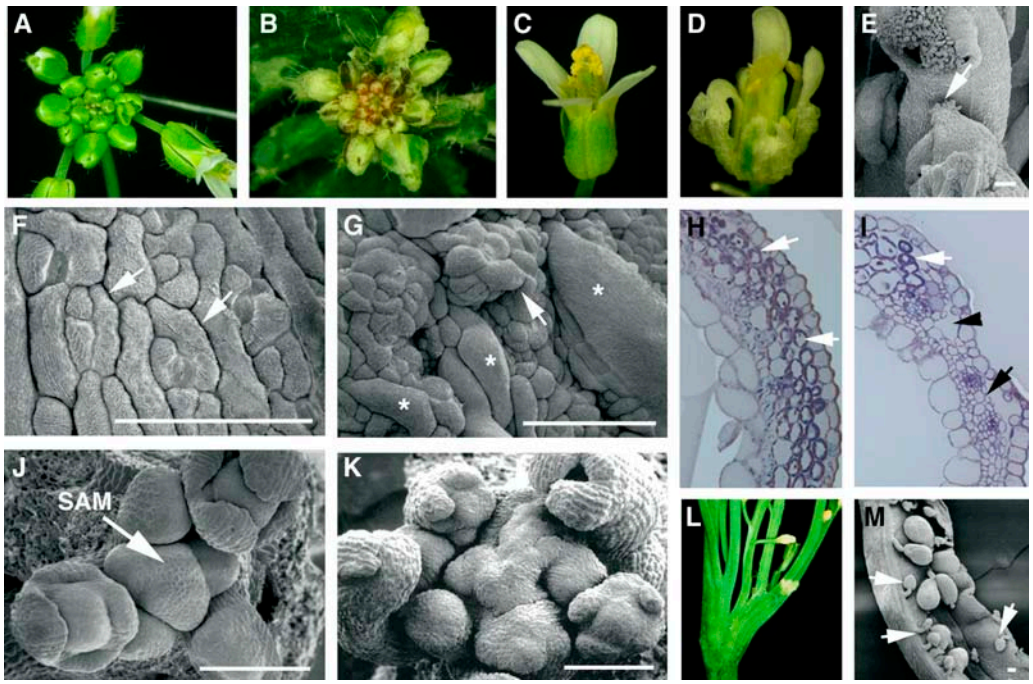

Figure 1. Phenotypic Analyses of Wild-Type and *tso2-1* Plants.

(A) A wild-type (L*er*) inflorescence.
(B) A *tso2-1* inflorescence showing white sectors on leaves and sepals.
(C) A wild-type flower.
(D) A *tso2-1* flower showing sepals with white sectors and rough surfaces.
(E) Partial homeotic transformation in a *tso2-1* floral organ, in which stigmatic tissues characteristic of carpels are found on top of an anther (arrow).
(F) Scanning electron micrograph of a wild-type sepal epidermis. Immature stomata (arrows) are interspersed with rectangular cells.
(G) A *tso2-1* sepal epidermis. Clusters of epidermal cells are projected above the epidermal surface, an example of which is indicated by the arrow. Some epidermal cells are significantly large and are marked with asterisks.
(H) Cross section of a wild-type carpel valve. Chloroplasts that encircle and outline the photosynthetic mesophyll cells are stained purple and are indicated by arrows.
(I) Cross section of a *tso2-1*/*tso2-1; rnr2b-1*/+ carpel valve. Although some mesophyll cells possess chloroplasts (white arrow), others completely lack chloroplasts (black arrow) and are small. Abnormal air spaces (black arrowhead) are present beneath the epidermis.
(J) Scanning electron micrograph of a wild-type SAM showing spiral arrangements of young floral primordia.
(K) A *tso2-1* SAM that is disorganized and is undergoing fasciation.
(L) A fasciated *tso2-1* plant showing multiple splits of the shoot.
(M) An open *tso2-1* silique showing mature seeds interspersed with aborted seeds or unfertilized ovules (arrows).
Bars = 100 μm.

and AY178109), the protein products of which are 70 and 90% identical, respectively, to TSO2. *RNR2B* is highly similar to *TSO2* even at the nucleic acid level, with 82% identity. *TSO2* and *RNR2B* also possess similar gene structures: *TSO2* has one small intron and *RNR2B* has no introns (Figure 2A). By contrast, *RNR2A* has a distinct gene structure, with eight introns and nine exons, and exhibits almost no sequence similarity to *TSO2* at the nucleic acid level, indicating that *RNR2A* probably has a distinct evolutionary origin from *TSO2* and *RNR2B*.

Interestingly, *RNR2B* from the Columbia (Col) accession possesses a 2-bp deletion resulting in a frameshift at Val-141 and a subsequent stop, deleting more than half of the protein, including 11 of the 16 invariant residues (Figure 2C). A second start codon could potentially direct the translational initiation of a second peptide homologous with TSO2 at residues 141 to 332 (Figure 2C). This putative second peptide does not have the N-terminal half of the protein containing 5 of the 16 invariant residues. Given the severity of the frameshift mutation in Col *RNR2B*, it is likely that it represents a loss-of-function or reduction-of-function allele. We thus named Col *RNR2B rnr2b-1*. Nevertheless, Col plants, which carry *rnr2b-1*, do not exhibit any obvious phenotype.

By contrast, *RNR2B* from L*er* and Wassilewskija (Ws) accessions (which are identical to each other) do not harbor the 2-bp deletion and differ from Col in 13 additional nucleotides (Figure 2C), resulting in an intact protein of 333 amino acid residues (AAO62422). To test whether L*er RNR2B* is a functional protein, *RNR2B* genomic DNA from L*er* (*RNR2B-L*) was fused to the strong and constitutive promoter 35S and transformed into the *tso2-1* mutant. This *35S:RNR2B-L* transgene was able to rescue all 36 *tso2-1* plants, indicating that the *RNR2B* gene from L*er* or Ws performs a function similar to *TSO2*.

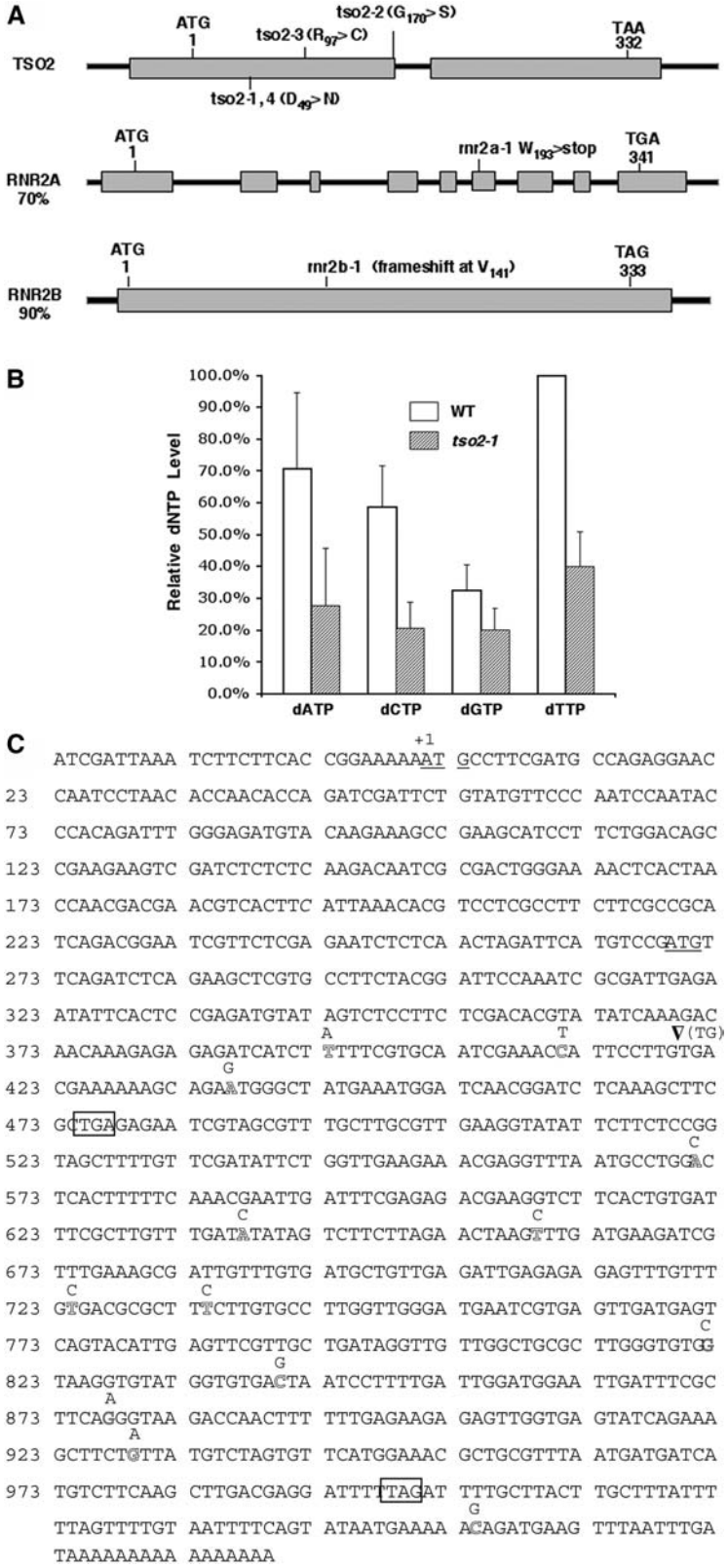

Figure 2. Functional Analyses of Three *Arabidopsis R2* Genes.

Previously, a cDNA encoding *RNR2A* was reported and its mRNA was shown to specifically accumulate during the S-phase of the cell cycle in synchronized tobacco BY2 cells (Philipps et al., 1995). We tested *RNR2A* function by fusing the *RNR2A* cDNA to the 35S promoter and transforming the construct into *tso2-1* mutants. The *35S:RNR2A* transgene was able to rescue the *tso2-1* phenotype in all 40 transgenic plants, indicating that *RNR2A* can substitute for *TSO2* when it is expressed from the strong and constitutive promoter. Using a reverse-genetics method known as TILLING (for targeting induced local lesions in genomes) (McCallum et al., 2000), we isolated an EMS-induced *rnr2a* mutation (*rnr2a-1*) in the Col accession. *rnr2a-1* is a nonsense mutation that deletes one-third of the RNR2A protein (Figure 2A). In the Col background, *rnr2a-1* is actually an *rnr2a-1 rnr2b-1* double mutant and is phenotypically wild-type (Figure 3A), indicating that *TSO2* alone provides sufficient *RNR* activity for normal development.

Aided by PCR-based markers specific to each mutant allele, we analyzed the F2 progeny of a cross between *tso2-1* (L*er*) and *rnr2a-1 rnr2b-1* (Col). *tso2-1 rnr2a-1* and *tso2-1 rnr2b-1* double mutants were identified, which exhibited a much stronger phenotype than either parent. First, *tso2-1 rnr2a-1* seedlings did not develop beyond the two- to four-leaf stage (Figure 3C). Their SAMs were terminated with callus-like cells (Figure 3D), and their leaves exhibited massively disorganized surfaces (Figures 3E and 3F). Second, *tso2-1 rnr2b-1* was embryo-lethal. PCR-based genotyping detected *tso2-1 rnr2b-1* only among aborted seeds, and not among viable plants from *tso2-1/tso2-1; rnr2b-1*/+ parents (Table 1). This finding strongly suggests that Col *RNR2B* (i.e., *rnr2b-1*) does not have any or does not have the same level of activity as the L*er RNR2B*. Finally, *tso2-1/tso2-1* plants heterozygous for *rnr2a-1*, *rnr2b-1*, or *rnr2a-1 rnr2b-1* were viable but exhibited a much stronger phenotype than *tso2-1/tso2-1*, as shown by their smaller stature, more severely reduced fertility, more frequent stem fasciation, and larger white sectors (Figures 3G to 3J). These results indicate that the functions of *RNR2A* and *RNR2B* are essential in the *tso2-1* background.

mRNA Expression Pattern of *TSO2*, *RNR2A*, and *RNR2B*

To test whether the *R2* genes exhibit different tissue- or stage-specific expression patterns, semiquantitative RT-PCR was performed for all three *R2* genes (Figure 4A). *TSO2* transcripts were found in roots, rosette and cauline leaves, stems, and flowers. Although *RNR2A* transcripts were not detected in roots, they were detected in rosette and cauline leaves, stems, and flowers. By contrast, *RNR2B* transcripts were detected only on DNA gel blots of RT-PCR products and were present in all tissues tested (Figure 4A, RNR2B.S). Thus, all three genes, in most cases, are expressed widely, with *RNR2B* expression at a much lower level than *TSO2* and *RNR2A*.

To examine *TSO2* transcription during the cell cycle, the β-glucuronidase (*GUS*) reporter gene was fused to the *TSO2* 1.2-kb promoter. Transgenic seedlings harboring *pTSO2:GUS* were treated with 5 μg/mL aphidicolin or 0.5% colchicine, which arrest cells at S- or M-phase, respectively. *GUS* expression was detected in more cells and at higher levels when the seedlings were arrested at S-phase (Figures 4B and 4C). By contrast, *GUS* expression was reduced dramatically when the seedlings were arrested at M-phase (Figure 4D). Hence, *TSO2* transcription occurs predominantly at the S-phase of the cell cycle.

TSO2 mRNA distribution during reproductive development was examined by in situ hybridization. The sporadic rather than uniform pattern of *TSO2* mRNA expression in developing floral tissues (Figures 4E and 4F) is characteristic of cell cycle phase–specific expression (Fobert et al., 1994). A large number of cells in the young floral meristem and developing floral organ primordia show a higher level of *TSO2* mRNA expression (Figure 4E). Cells in the developing ovules and carpel valves also express *TSO2* mRNA at a high level (Figure 4F). Therefore, the *TSO2* mRNA expression pattern is consistent with its role in dNDP biosynthesis during DNA replication in actively dividing cells.

tso2-1 Exhibits Defects in Cell Cycle Progression

Because yeast *rnr* mutants display a *cdc* phenotype, we tested whether cell cycle progression is affected in *tso2-1* mutants. In situ hybridization examining the expression of cell cycle phase–specific markers was performed. G2/M-specific *Cyclin B1* (*CycB1*) and S-specific *Histone4* (*H4*) expression was examined in wild-type and *tso2-1* floral tissues. *CycB1* and *H4* were both expressed strongly in a sporadic manner in wild-type as well as *tso2-1* tissues (Figures 5A to 5D). Although the *CycB1* expression pattern was similar in the wild type and *tso2-1*, *H4* expression was significantly different between the wild type and *tso2-1*. Many more cells in *tso2-1* inflorescences expressed *H4* than in the wild type, suggesting a prolonged S-phase in these *tso2-1* cells. We also examined *CycB1* and *H4* expression in *tso2-1 rnr2a-1* seedlings (Figures 5E to 5H). Although wild-type seedlings expressed both *CycB1* and *H4* strongly in the SAM and

Figure 2. (continued).

(A) Scheme of three *Arabidopsis R2* genes. Rectangular boxes represent exons. The start and stop codons and the position of each *r2* mutation are indicated. *tso2-1* and *tso2-4* are identical. Numbers indicate amino acid residues. Percentage identities between *TSO2* and *RNR2A* or *RNR2B* are indicated.

(B) Relative dNTP levels in wild-type (L*er*) and *tso2-1* floral tissues. Results from three different experiments were averaged and normalized to the wild-type dTTP level. Error bars represent SD.

(C) Full-length *RNR2B* cDNA sequence from Col (BT004167). Two start codons are underlined, and two stop codons are boxed. The L*er RNR2B* sequence differs from the Col sequence at 14 positions, which are indicated immediately above the corresponding Col positions. An arrowhead indicates a 2-bp (TG) deletion from Col resulting in premature translational termination at the first stop codon. A second start codon could potentially direct the translational initiation of a second peptide. Single base pair changes at positions 659, 734, 822, 840, and 929 are missense, but the remaining single base pair changes are silent. The *RNR2B* sequence from the Ws accession is identical to that of L*er*.

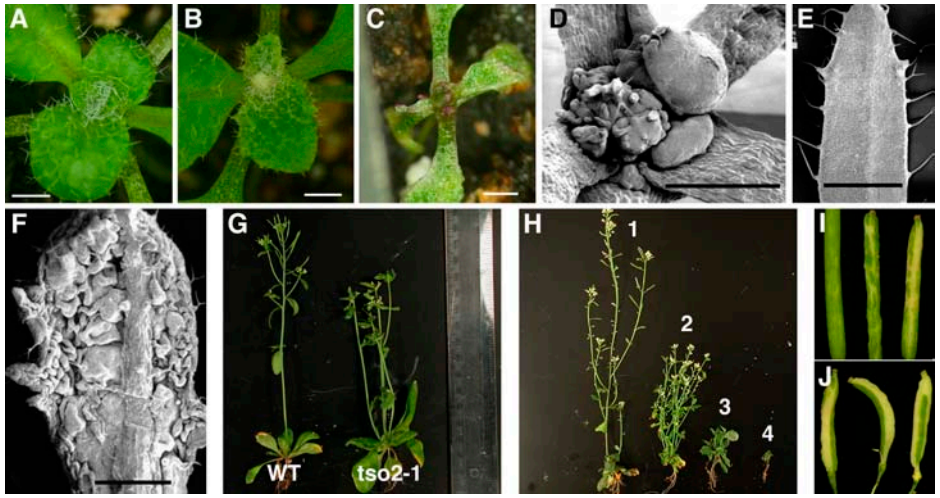

Figure 3. Phenotypes of *r2* Single and Double Mutants.

(A) An *rnr2a-1 rnr2b-1* seedling showing no obvious phenotype.
(B) A *tso2-1* seedling. White tissues are forming in the emerging leaves.
(C) A typical *tso2-1 rnr2a-1* seedling, which will not develop further.
(D) The SAM of a *tso2-1 rnr2a-1* seedling that terminates with callus-like cells.
(E) A wild-type leaf.
(F) A *tso2-1 rnr2a-1* leaf showing a severely disrupted leaf surface.
(G) A wild-type L*er* plant and a *tso2-1* plant.
(H) Six-week old *tso2-1/tso2-1* plants singly or doubly heterozygous for *rnr2a-1* and/or *rnr2b-1*: *tso2-1/tso2-1* (1); *tso2-1/tso2-1; rnr2b-1/+* (2); *tso2-1/tso2-1; rnr2a-1/+* (3); and *tso2-1/tso2-1; rnr2a-1/+; rnr2b-1/+* (4).
(I) *tso2-1* siliques showing small white sectors in the green carpel valve.
(J) *tso2-1/tso2-1; rnr2b-1/+* siliques showing larger white sectors and smaller siliques.
Bars in **(A)** to **(F)** = 1 mm.

developing leaves, *tso2-1 rnr2a-1* seedlings possessed little or no *CycB1*- or *H4*-expressing cells, perhaps because of a complete absence of cell division activity in *tso2-1 rnr2a-1* seedlings.

DNA Damage Accumulation in *tso2-1 rnr2a-1*

Are the reduced dNTP levels in *tso2-1* sufficient to impede DNA replication fork progression and induce DNA strand breaks? Using the comet assay (Angelis et al., 1999), we measured DNA damage levels in 2-week-old seedlings of *tso2* single and double mutants. Although *tso2-1* or *rnr2a-1 rnr2b-1* did not exhibit increased DNA damage, *tso2-1 rnr2a-1* exhibited significant increases in DNA damage (Figure 6A). Furthermore, the DNA damage level in 5-week-old *tso2-1 rnr2a-1* seedlings was much higher than that in 2-week-old *tso2-1 rnr2a-1* seedlings.

Consistent with the comet assay, only *tso2-1 rnr2a-1* seedlings were found to induce the expression of molecular markers associated with DNA damage repair (Figure 6B). These markers included poly(ADP-ribose) polymerase1 (*ATPARP1*), *ATPARP2*, and *ATRAD51* (Doutriaux et al., 1998; Doucet-Chabeaud et al., 2001). Both *ATPARP1* and *ATPARP2* are transcriptionally induced by increased levels of double-stranded DNA breaks. However, *ATPARP2* can also be induced by oxidative stresses. *ATRAD51* is involved in meiotic recombination and in homologous recombination repair and is induced by increased double-stranded DNA breaks (Osakabe et al., 2002). The induction of *ATPARP1*, *ATPARP2*, and *ATRAD51* contrasts sharply with the nearly complete shutdown of *CycB1* and *H4* expression in *tso2-1 rnr2a* seedlings (Figures 5F and 5H), suggesting that *tso2-1 rnr2a-1* double mutants did not simply shut down transcription machinery altogether but were able to selectively induce DNA repair genes.

Increased Sensitivity to UV-C Light in *tso2-1* and *tso2-1 rnr2a-1* Seedlings

Because RNR also provides dNTPs for DNA damage repair, the reduced dNTP pool sizes in *tso2-1* might lead to hypersensitivity to DNA-damaging agents. We tested the sensitivity of wild-type (L*er*), *tso2-1*, *rnr2a-1 rnr2b-1*, and *tso2-1 rnr2a-1* seedlings to

Table 1. Results of Genotyping among the Progeny of *tso2-1/tso2-1; rnr2b-1/+* Parents

	rnr2b-1/rnr2b-1	*rnr2b-1/+*	*+/+*	Total
Number of plants				
Expected	9	18	9	36
Observed	0	22	14	36
Number of seeds				
Green (normal)	0	13	5	18
White (abnormal)	2	33	3	38

Only the genotype at *RNR2B* is shown, as all plants are also *tso2-1/tso2-1*.

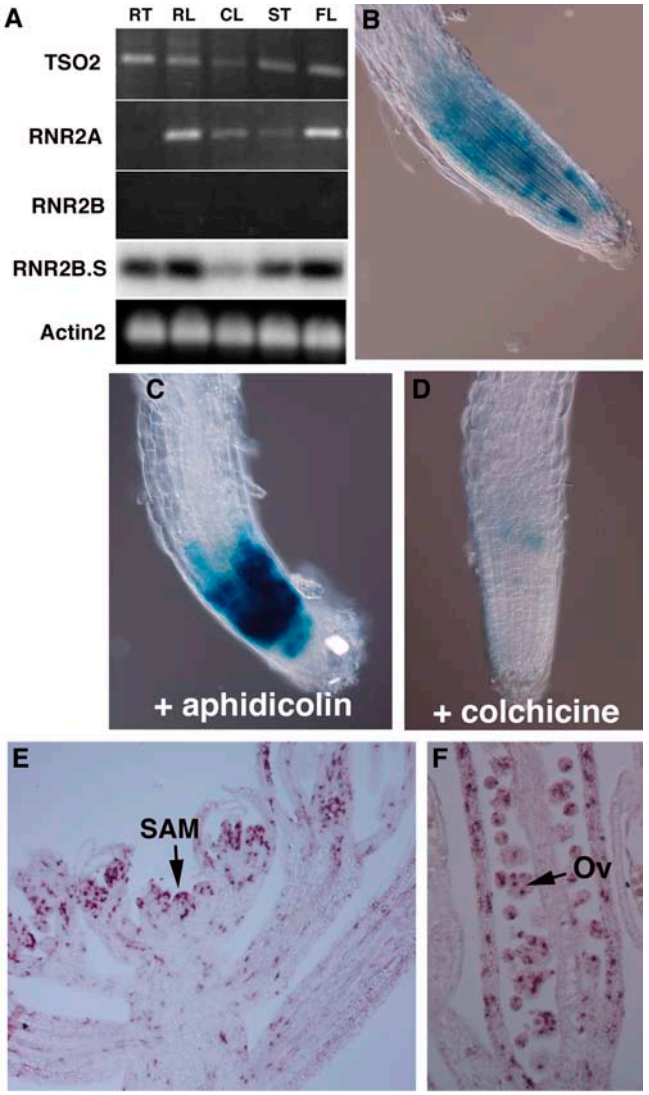

Figure 4. mRNA Expression of *TSO2*, *RNR2A*, and *RNR2B*.

(A) Expression of *TSO2*, *RNR2A*, and *RNR2B* mRNA measured by 20 cycles of RT-PCR with gene-specific primers. RT, root; RL, rosette leaves; CL, cauline leaves; ST, stems; FL, flowers. The RT-PCR products of *RNR2B* were detected only by DNA gel blot hybridization with a *RNR2B*-specific probe (lane RNR2B.S). *Actin2* was the loading control.
(B) *pTSO2*:*GUS* expression in a 3-d-old wild-type root. Note the sporadic GUS activity.
(C) *pTSO2*:*GUS* expression in a 3-d-old root treated with 5 μg/mL aphidicolin, revealing an increased number of *GUS*-expressing cells and an increased level of *GUS* expression.
(D) *pTSO2*:*GUS* expression in a 3-d-old root treated with 0.5% colchicine. Note the significantly reduced *GUS* activity.
(E) In situ hybridization showing *TSO2* mRNA expression in a wild-type L*er* SAM. Note the sporadic *TSO2* expression throughout the young floral primordia.
(F) In situ hybridization showing sporadic *TSO2* expression in developing ovules (Ov) and carpel valves.

UV-C light (Figure 7A). *tso2-1 rnr2a-1* exhibited significantly increased sensitivity to UV-C light. *tso2-1* exhibited slightly increased sensitivity to UV-C light, but only at high UV-C light levels. *rnr2a-1 rnr2b-1* exhibited a level of UV-C light sensitivity similar to the wild type (L*er*), indicating that *TSO2* alone is sufficient to provide wild-type levels of protection against UV-C light.

Release of TGS in *tso2-1 rnr2a-1*

The phenotype of *tso2-1* associated with meristem fasciation and increased sensitivity to DNA-damaging agents resembles that of several *Arabidopsis* mutants defective in DNA/chromatin replication and assembly, including mutants of *BRU1*, *FAS1*, *FAS2*, *ATCAP-E1*, *ATCAP-E2*, and *ATMRE11* (Kaya et al., 2001; Bundock and Hooykaas, 2002; Siddiqui et al., 2003; Takeda et al., 2004). All of these mutants were found to release TGS (Kaya et al., 2001; Takeda et al., 2004) at the pericentromeric repeats called *Transcriptional Silent Information* (*TSI*) (Steimer et al., 2000). We found that *tso2-1 rnr2a-1* seedlings also released silencing at *TSI* but *tso2-1* seedlings did not (Figure 7B). Because *tso2-1* plants exhibit more severe mutant phenotypes at reproductive stages, we tested *tso2-1* inflorescence tissues for the release of *TSI*. No *TSI* expression was observed in *tso2-1* inflorescence tissues (data not shown).

PCD in *tso2-1 rnr2a-1*

In animals, genomic instability often induces PCD in a p53-dependent manner (Chernova et al., 1995; Vogelstein et al., 2000). Furthermore, apoptosis was reported to occur in p53R2 knockout mice (Kimura et al., 2003). Therefore, we tested whether the accumulating DNA damage in *tso2-1 rnr2a-1* seedlings described above could lead to PCD using histochemical markers. Trypan blue was used to stain dead cells (Rate et al., 1999). Large patches of trypan blue–stained cells were observed in the leaves of 10-d-old *tso2-1 rnr2a-1* seedlings but not in wild-type or *tso2-1* seedlings (Figure 8; data not shown). Furthermore, a high level of H_2O_2 and a large number of callose depositions were detected in the leaves of 10-d-old *tso2-1 rnr2a-1* seedlings (Figure 8). Both H_2O_2 production and callose deposition are indicators of plant cells undergoing hypersensitive PCD during incompatible plant–pathogen interactions (Dietrich et al., 1994; Brodersen et al., 2002), suggesting that the cell death observed in *tso2 rnr2a* is likely programmed.

To further characterize *tso2 rnr2a*–mediated PCD, the first two leaves of 3-week-old wild-type (L*er*) and *tso2-1 rnr2a-1* plants were fixed, sectioned, and processed for terminal deoxyribonucleotidyl transferase–mediated dUTP nick-end labeling (TUNEL). TUNEL can sensitively detect DNA fragmentation, one of the hallmarks of PCD, by labeling exposed 3′ hydroxyl ends of DNA fragments with fluorescein-dUTP. The same leaf sections were simultaneously stained with 4′,6-diamidino-2-phenylindole (DAPI) to reveal all nuclei in each section (Figures 9A, 9C, and 9F). None of the nuclei in wild-type sections was TUNEL-positive (Figure 9B). By contrast, some but not all nuclei in *tso2-1 rnr2a-1* leaf sections were TUNEL-positive (Figures 9C and 9D), indicating that not all cells in *tso2-1 rnr2a-1* leaves had undergone PCD. Some TUNEL-positive nuclei in *tso2-1 rnr2a-1* leaves exhibited

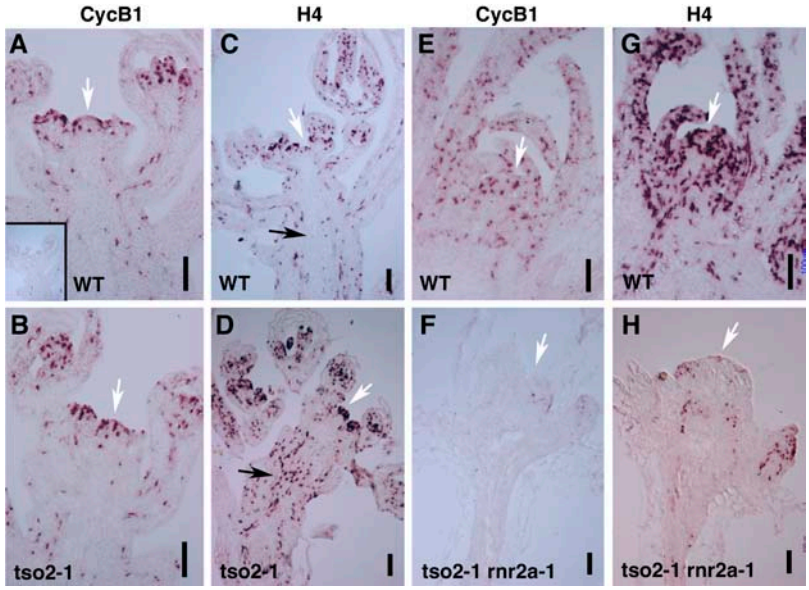

Figure 5. In Situ Hybridization Examining the Expression of Cell Cycle Phase–Specific Marker Genes.

(A) *CycB1* mRNA expression in wild-type SAM and developing young flowers. The white arrow indicates the SAM. The inset shows a wild-type SAM hybridized with the sense *CycB1* RNA probe as a negative control.
(B) *CycB1* expression in *tso2-1* SAM and young flowers.
(C) *H4* expression in a wild-type inflorescence. The black arrow indicates a lack of *H4*-expressing cells in the stem.
(D) *H4* expression in a *tso2-1* inflorescence. A dramatic increase in H4-expressing cells in flowers and in the stem (black arrow) is evident.
(E) *CycB1* RNA expression in a wild-type 3-week-old seedling.
(F) *CycB1* RNA expression in a 3-week-old *tso2-1 rnr2a-1* seedling.
(G) *H4* expression in a wild-type 3-week-old seedling.
(H) *H4* expression in a 3-week-old *tso2-1 rnr2a-1* seedling.
Bars = 10 μm.

nuclear morphologies characteristic of apoptotic nuclei, including marginalization of chromatin on the nuclear membrane, fragmentation of the nucleus into small bodies, and peripheral nuclear crescents (Figures 9E and 9H to 9J). The apoptotic nuclear morphology provides the most convincing evidence for the occurrence of PCD in the *tso2 rnr2a* mutants, as DNase I–treated nuclei in wild-type leaf sections fail to show apoptotic nuclear morphology even though they are TUNEL-positive (Figure 9K). This observation is consistent with other published work (Kressel and Groscurth, 1994), indicating that TUNEL labeling can only be considered specific for PCD when it is associated with the characteristic nuclear morphology.

Does the DNA damage occur before the initiation of the apoptosis-like PCD in these *tso2-1 rnr2a-1* seedlings? DNA damage was already shown to occur in 2- and 5-week-old *tso2-1 rnr2a-1* seedlings (Figure 6A). Subsequently, 6-d-old seedlings were also tested for DNA damage using the comet assay. The 6-d-old *tso2-1 rnr2a-1* seedlings showed 52% (±10% SE) more relative DNA damage units than the corresponding wild-type seedlings, indicating DNA damage accumulation in the 6-d-old *tso2-1 rnr2a-1* seedlings. The TUNEL assay was then used to determine the time course of cell death in *tso2-1 rnr2a-1* at 6, 11, and 16 d after germination. Although none of the 8-μm sections of 6-, 11-, and 16-d-old wild-type seedlings (including cotyledon and hypocotyls) was TUNEL-positive (data not shown), the *tso2-1 rnr2a-1* seedling sections showed increased TUNEL signals with age. Specifically, the majority of the 6-d-old *tso2-1 rnr2a-1* seedling sections was negative for the TUNEL signal (Figures 9L and 9M). By examining 200 sections, only an average of fewer than one (0.62; $n = 200$) TUNEL-positive nucleus per section was observed. At 11 d, an increased average number (1.8; $n = 160$) of TUNEL-positive nuclei per section was observed (Figures 9N and 9O). At 16 d, an average of 6.7 ($n = 180$) TUNEL-positive nuclei per section was observed. However, none of the TUNEL-positive nuclei in 6- and 11-d-old seedlings exhibited the apoptotic nuclear morphology (Figures 9L to 9O). Apoptotic nuclear morphology was observed starting in 16-d-old *tso2 rnr2a* seedlings (data not shown) and continuing in 3-week-old *tso2 rnr2a* seedlings (Figures 9E and 9H to 9J). Therefore, DNA damage was detected at least 10 d before the appearance of nuclei exhibiting characteristic apoptotic morphology in the *tso2-1 rnr2a-1* seedlings.

To date, PCD in plants has been studied extensively in the context of the hypersensitive response (HR) during incompatible plant–pathogen interactions and senescence (Greenberg, 1996; Kuriyama and Fukuda, 2002; Greenberg and Yao, 2004). PCD during senescence is often accompanied by a rapid loss of chlorophyll and reduced expression of photosynthesis-associated genes (PAGs), such as chlorophyll *a/b* binding protein (CAB1 and CAB2) and ribulose-1,5-bis-phosphate carboxylase/oxygenase

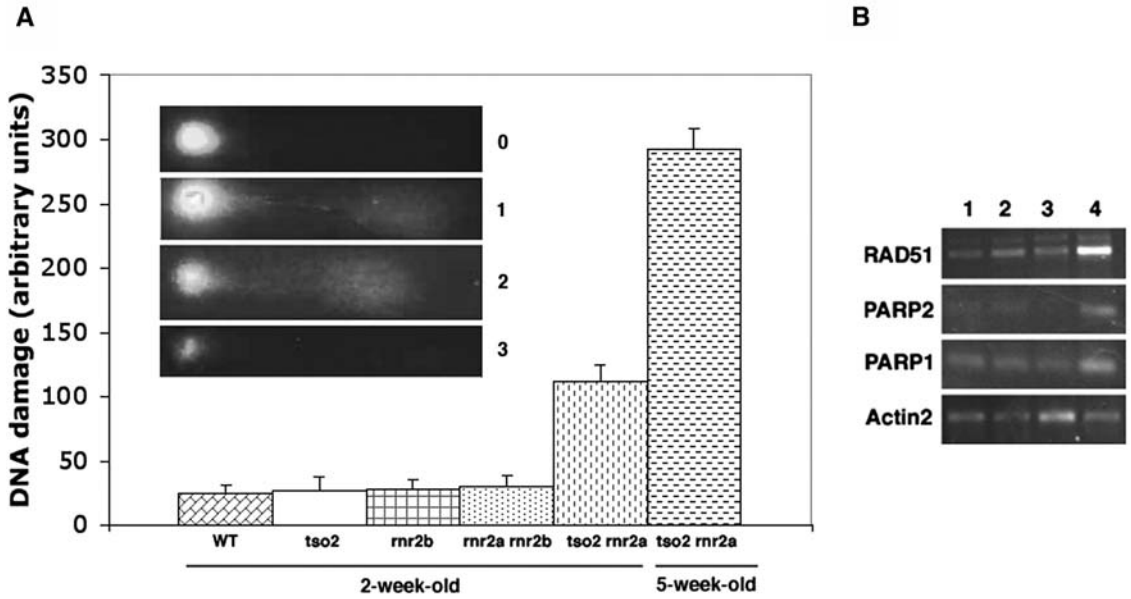

Figure 6. Increased DNA Damage in *tso2-1 rnr2a-1* Seedlings.

(A) Results from the comet assay indicating the relative amount of DNA damage in different genotypes. Although *tso2-1*, *rnr2b-1*, or *rnr2a-1 rnr2b-1* mutants exhibited levels of DNA damage similar to those in the wild type (L*er*), *tso2-1 rnr2a-1* double mutants exhibited an increased level of DNA damage even at 2 weeks old. The DNA damage level was increased further in 5-week-old *tso2-1 rnr2a-1* plants. The extent of DNA damage in each nucleus is indicated by the units 0, 1, 2, 3, or 4. An increased unit correlated with a larger comet tail and a smaller comet head, as illustrated in the inset. The DNA damage units per genotype were derived by summing the units from 100 nuclei on each slide. Error bars represent SD values averaged from four slides.

(B) Twenty-seven to 30 cycles of RT-PCR were used to detect the induction of *ATPARP1*, *ATPARP2*, and *ATRAD51* in 3-week-old seedlings. Lanes 1, 2, 3, and 4 correspond to the wild type (L*er*), *tso2-1*, *rnr2a-1 rnr2b-1*, and *tso2-1 rnr2a-1*, respectively.

small subunit (RbcS) (Miller et al., 1999). To test whether *tso2 rnr2a*–mediated PCD is caused by early senescence, we examined the expression of the PAGs CAB1, CAB2, and RbcS in 3-week-old seedlings of the wild type (L*er*), *tso2-1*, *rnr2a-1 rnr2b-1*, and *tso2-1 rnr2a-1* by semiquantitative RT-PCR (Figure 10A). All genotypes were similar to the wild type in expressing the three PAGs, in contrast with what would have been expected if *tso2 rnr2a* had undergone early senescence. In addition, we tested the expression of genes previously shown to be associated with HR-mediated PCD in plants (Brodersen et al., 2002), including *Senescence-Associated Gene13* (*SAG13*), *Peroxidase Cb* (*PRXcb*), *Glutathionine-S-Transferase11* (*GST11*), *Pathogenesis-Related1* (*PR1*), and *Enhanced Disease Susceptibility1* (*EDS1*). Additionally, *SAG12*, a Cys protease specific to senescence-induced PCD (Pontier et al., 1999), was tested. Using RT-PCR, we compared the expression of these genes in the wild type (L*er*) and *tso2-1 rnr2a-1* (Figure 10B). Although the expression of *SAG13*, *GST11*, and *EDS1* was induced, the expression of *SAG12* was not detected under the RT-PCR conditions used. Overall, *tso2 rnr2a*–mediated PCD appears similar to HR-mediated PCD in plants.

DISCUSSION

Our molecular genetic studies of *tso2* led to the identification and characterization of all three *RNR2* genes in the *Arabidopsis* genome. The analyses of single and double *rnr2* mutants demonstrated that normal dNTP pool and RNR function are critical for the plant response to mutagens and for proper plant development. Interestingly, although all four *tso2* missense alleles exhibited morphological defects, single *rnr2a-1* and *rnr2b-1* and double *rnr2a-1 rnr2b-1* mutants did not. It is likely that *TSO2* normally plays a more predominant role than *RNR2A* and *RNR2B*. This is supported by the Affymetrix gene expression profiling study at AtGenExpress (Schmid et al., 2005), which shows that *TSO2* is more abundantly and widely expressed than *RNR2A*, and by a recent transcriptome profiling study showing a 10-fold induction of *TSO2* transcripts upon treatment with the genotoxins bleomycin plus mitomycin C (Chen et al., 2003). It is also possible that the four *tso2* missense alleles are recessive antimorphic alleles. Recessive antimorphism is possible if the mutant TSO2 proteins interact with R1 or other R2 subunits, inactivating R1 or other R2 subunits. But this negative effect is masked by the wild-type TSO2 protein.

Although *tso2* single mutants are viable, the *tso2 rnr2a* and *tso2 rnr2b* double mutants are seedling- and embryo-lethal, respectively, suggesting that both *RNR2A* and *RNR2B* function are essential in the *tso2* mutant background. Interestingly, *tso2 rnr2a* seedlings exhibited a range of phenotypes not observed in *tso2* single or *rnr2a rnr2b* double mutants, including the loss of *CycB1* and *H4* expression (Figures 5F and 5H), DNA damage accumulation (Figure 6), a high degree of UV-C light sensitivity (Figure 7A), release of TGS (Figure 7B), and PCD (Figures 8 and

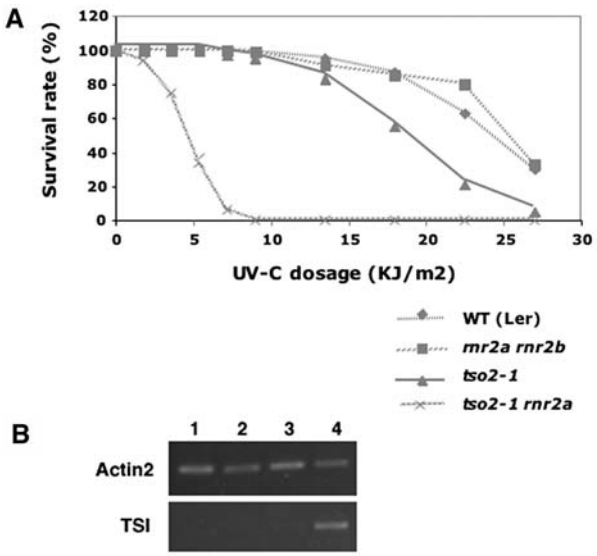

Figure 7. Increased Sensitivity to UV-C Light and Epigenetic Misregulation in *r2* Mutants.

(A) Graph illustrating the survival rate of wild-type (L*er*), *tso2-1*, *rnr2a-1 rnr2b-1*, and *tso2-1 rnr2a-1* seedlings under increasing UV-C light levels.
(B) Twenty-five cycles of RT-PCR were used to detect *TSI* transcripts in 3-week-old seedlings. Lanes 1, 2, 3, and 4 correspond to the wild type (L*er*), *tso2-1*, *rnr2a-1 rnr2b-1*, and *tso2-1 rnr2a-1*, respectively.

9). It is likely that a greater degree of reduced or imbalanced dNTP pool in *tso2 rnr2a* could lead to greater DNA replication block and DNA damage, triggering subsequent phenotypes such as the release of TGS and PCD. However, the *tso2 rnr2a* double mutants did not just deregulate all genes nonspecifically. For example, the photosynthesis-associated genes CAB1, CAB2, and RbcS are expressed at a level similar to that in the wild type (Figure 10A). In addition, although the cell cycle genes *CycB1* and *H4* are turned off (Figures 5F and 5H), the DNA damage repair genes *ATPARP1*, *ATPARP2*, and *ATRAD51* are specifically induced in *tso2 rnr2a* seedlings (Figure 6B). The identification and construction of single and double *r2* mutants offer the opportunity to study the diverse functions of RNR in plant development.

Decreased dNTP Levels Affect Organelle Replication

One unique feature of *tso2* mutants is the formation of white sectors on green organs. We observed a lack of chloroplasts in the photosynthetic mesophyll cells, unusual air spaces beneath the epidermis, and abnormally small mesophyll cells in *tso2* tissues (Figures 1H and 1I). In yeast, lower RNR activity or reduced dNTP level was shown to increase the formation of mitochondrial DNA–deficient cells (petite cells) (Zhao et al., 1998, 2001), suggesting that organelle DNA replication is highly sensitive to reduced dNTP levels. Therefore, stochastic depletions of chloroplasts and/or mitochondria may underlie the white sectors and small cells in *tso2* mutants. The development of white sectors occurring in the fifth leaf and in later-arising organs of *tso2* could result from a gradual dilution of dNTP, which may be highly enriched in embryos/seedlings via salvage pathways (Reichard, 1988; Saada et al., 2001).

Defects in TGS May Underlie the Developmental Defects of *tso2*

Previous research has suggested that stochastic release of TGS in *bru1* and *fas* mutants caused meristem fasciation as a result of the ectopic expression of *WUSCHEL* (*WUS*), a key meristem regulator (Mayer et al., 1998; Kaya et al., 2001; Takeda et al., 2004). Here, we showed that *tso2-1 rnr2a-1* exhibited defects in epigenetic inheritance by releasing silencing at the *TSI* locus, suggesting that the fasciated SAM and homeotic transformation of floral organs observed in *tso2-1* could be caused by stochastic release of silencing at loci including *WUS* and *AGAMOUS*. Because we

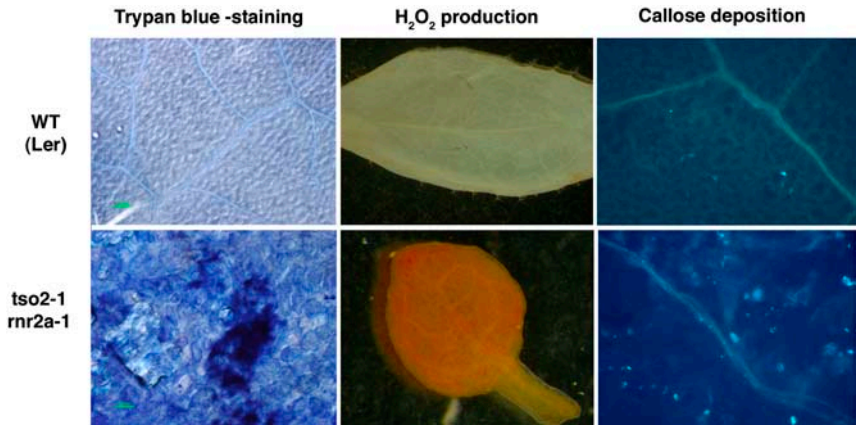

Figure 8. Expression of Cell Death Markers in *tso2-1 rnr2a-1* Mutants.

Rosette leaves of 10-d-old wild-type and *tso2-1 rnr2a-1* plants were examined for PCD using three different histochemical markers: trypan blue staining, H_2O_2 production, and callose deposition. Dark blue patches stained by trypan blue, reddish-brown deposits (reaction products between 3,3-diaminobenzidine and H_2O_2), and callose deposition revealed by aniline blue staining indicated PCD in *tso2-1 rnr2a-1* mutants.

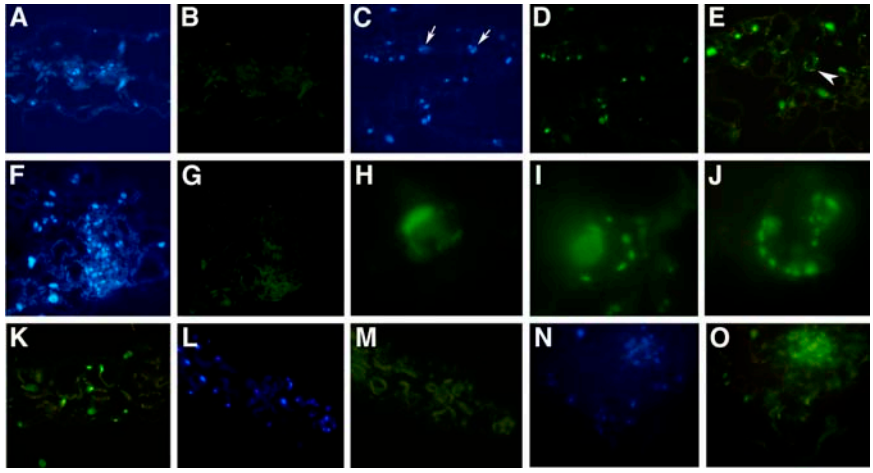

Figure 9. PCD in *tso2-1 rnr2a-1* Double Mutants Detected by the TUNEL Assay.

Images shown in **(A)** to **(K)** are from 3-week-old seedlings. Images shown in **(L)** and **(M)** and in **(N)** and **(O)** are from 6- and 11-d-old seedlings, respectively. Images in **(A)** to **(G)** and **(K)** to **(O)** are magnified ×88. Images in **(H)** to **(J)** are magnified ×366.

(A) DAPI staining of nuclei in a wild-type (L*er*) leaf section.

(B) The same wild-type leaf section shown in **(A)** is TUNEL-negative, showing no green fluorescent signal.

(C) DAPI staining of nuclei in a *tso2-1 rnr2a-1* leaf section.

(D) Many TUNEL-positive (green fluorescent) nuclei are found in the same *tso2-1 rnr2a-1* leaf section shown in **(C)**. Some nuclei (indicated by arrows in **[C]**) are not fluorescent, indicating that some cells have not undergone PCD.

(E) TUNEL-positive nuclei in a *tso2-1 rnr2a-1* leaf section. Nuclear morphologies characteristic of different stages of PCD are shown. The arrowhead indicates a cell enlarged in **(J)**.

(F) DAPI staining of nuclei in a *tso2-1 rnr2a-1* leaf section.

(G) A negative control for the TUNEL. The same leaf section shown in **(F)** was not provided with terminal deoxyribonucleotidyl transferase during TUNEL labeling.

(H) A TUNEL-positive nucleus in a *tso2-1 rnr2a-1* leaf section. The crescent-shaped nuclear morphology was previously described for UV-C light–treated protoplast cells undergoing PCD (Danon and Gallois, 1998).

(I) A TUNEL-positive nucleus of *tso2-1 rnr2a-1* exhibiting marginalization of chromatin on the nuclear membrane and fragmentation of the nucleus into small bodies.

(J) An enlargement of the TUNEL-positive nucleus shown in **(E)** showing fragmented DNA bodies at the nuclear peripheral.

(K) A wild-type (L*er*) leaf section treated with DNase I before detection by the TUNEL. The DNA nicks created by DNase I give positive TUNEL signals. However, none of the TUNEL-positive nuclei exhibit apoptotic characteristics, as shown in **(H)** to **(J)**.

(L) DAPI staining of nuclei in a cotyledon section of a 6-d-old *tso2-1 rnr2a-1* seedling.

(M) An absence of TUNEL-positive nuclei in the same cotyledon section shown in **(L)**. Chloroplasts are visible as a result of their autofluorescence.

(N) DAPI staining of nuclei in a cotyledon section of an 11-d-old *tso2-1 rnr2a-1* seedling.

(O) TUNEL-positive nuclei in the same cotyledon section shown in **(N)**.

failed to detect *TSI* in *tso2-1* single mutants, it is possible that stochastic release of *TSI* or other regulatory genes is rare and difficult to detect in *tso2-1*. Future in situ hybridization experiments will be necessary to determine whether *tso2-1* single mutants also exhibit defects in TGS. To date, there are no reports of defects in TGS in *rnr* mutants of yeast or mammals. It remains to be seen whether release of TGS could be the underlying basis of the growth abnormalities in *rnr* mutants of fungi or animals.

In addition to meristem fasciation and homeotic transformation of floral organs, *tso2-1* mutants exhibited additional developmental defects, such as disorganized leaf cell layers (Figure 1I), aborted seed development (Figure 1M), unfused carpels (Figure 1E), and the formation of multiple carpels (data not shown). These developmental defects may be caused by additional mechanisms other than epigenetic misregulation. For example, the delayed cell division cycle shown by the significant increase in *H4*-expressing cells in *tso2-1* (Figure 5) could lead to altered cell-to-cell communication, which is essential for proper organ fusion or proper cell layer organization. Alternatively, RNR may have additional functions not limited to the simple production of DNA building blocks (Chabes and Thelander, 2003). Downes et al. (2000) suggested that the normally high levels of intracellular purine dNDPs at S-phase act as an intracellular signal for the S-phase, retarding the progression toward M-phase. This may explain why RNR is more involved in oncogenic transformation than is expected for a simple metabolic enzyme (Downes et al., 2000).

tso2-1 rnr2a-1 Undergoes PCD

We demonstrated that cells in *tso2-1 rnr2a-1* seedlings underwent PCD. Histochemical markers, molecular markers, and the TUNEL assay were used to analyze the cell death that occurred in *tso2-1 rnr2a-1* double mutants. The nuclear morphology combined with the positive TUNEL signal indicative of DNA

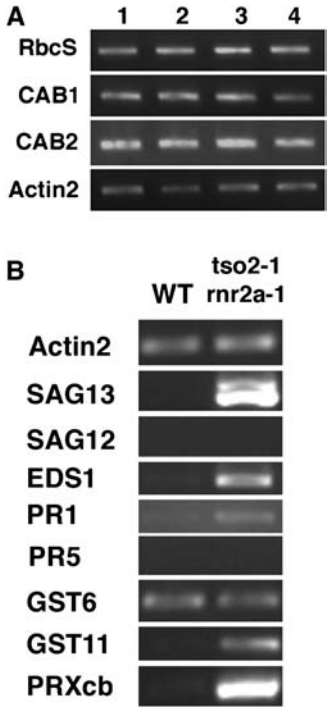

Figure 10. Expression of Molecular Markers Associated with Senescence and HR-Mediated PCD.

(A) RT-PCR was used to examine photosynthesis-associated genes. Twenty, 27, and 17 PCR cycles were used to examine *RbcS*, *CAB1*, and *CAB2*, respectively. *Actin2* was the loading control. Lanes 1, 2, 3, and 4 correspond to 3-week-old seedlings of the wild type (L*er*), *tso2-1*, *rnr2a-1 rnr2b-1*, and *tso2-1 rnr2a-1*, respectively.

(B) Twenty-five cycles of RT-PCR were used to detect molecular markers associated with PCD in 3-week-old seedlings. *SAG13*, *EDS1*, *PR-1*, *GST11*, and *PRXcb* were induced to various levels in *tso2-1 rnr2a-1* mutants. *GST6* remained the same in both the wild type and *tso2-1 rnr2a-1*. *SAG12* and *PR-5* were not induced. However, *SAG12* could be detected using 30 cycles of PCR (data not shown). A doublet was amplified with the *SAG13* primers as a result of a nearly identical gene (At2g29350) encoding tropinone reductase. *SAG13* corresponds to the upper band of the doublet.

fragmentation provided strong support for the occurrence of apoptosis-like PCD in *tso2 rnr2a* mutants. Our data also revealed that the PCD in *tso2 rnr2a* plants resembles HR-mediated PCD with regard to histochemical markers and gene expression, suggesting that although the triggers of PCD may differ in *tso2 rnr2a*, many of the downstream effector genes of PCD may be shared among different PCD pathways in higher plants.

Possible Mechanisms Triggering PCD in *tso2 rnr2a*

What could be the trigger for PCD in *tso2 rnr2a* double mutants? In mammalian cells, DNA damage switches on the tumor-suppressor protein p53, which induces cell cycle arrest and PCD (apoptosis) (Chernova et al., 1995; Vogelstein et al., 2000). Whether PCD occurs in response to DNA damage as a defense mechanism in plants remains unresolved. A p53 homolog has not been identified in plants, even though the entire genome of *Arabidopsis* has been sequenced. Moreover, PCD was not detected in telomerase-deficient lines (Riha et al., 2001), and many mutants defective in DNA repair, such as mutants of the single-copy *Arabidopsis* gene *KU80*, are viable and wild type–like under normal growth conditions (West et al., 2002). However, fragmented nuclei resembling apoptotic nuclei have been mentioned in *Arabidopsis* mutants of *ATTOP6B*, which encodes a homolog of archaebacterial topoisomerase subunit B (Hartung et al., 2002). Nuclear degradation in aphidicolin-treated *ataxia telangiectasia-mutated* and *rad3-related* mutant cells was also reported (Culligan et al., 2004). A more in-depth characterization of UV light–induced PCD was performed using *Arabidopsis* protoplast cells (Danon and Gallois, 1998). The UV-C light–induced PCD was shown to be mediated by a caspase-like activity, as it can be suppressed by the caspase inhibitor p35 and *Defender Against apoptotic Death* (Danon et al., 2004). Because the UV irradiation could cause damage to other cellular components, whether DNA damage could directly induce PCD in plant cells is still debatable. If a p53-related pathway exists in plants, as suggested by Whittle et al. (2001), the p53-like gene might have little sequence homology with its mammalian counterpart.

Could the DNA damage accumulated in *tso2 rnr2a* double mutants directly trigger PCD? Among all *r2* single and double mutants examined, only the *tso2 rnr2a* double mutants accumulated DNA damage and only *tso2 rnr2a* exhibited PCD. The correlation between DNA damage and PCD in *tso2 rnr2a* suggests that the DNA damage in *tso2 rnr2a* may trigger these cells to undergo PCD to eliminate damaged cells. This suggestion is further supported by the time course analyses, which revealed DNA damage accumulation occurring at least 10 d before the appearance of apoptotic nuclei in the *tso2 rnr2a* seedlings (Figure 9). By examining whether PCD occurs in other plant mutants defective in genome integrity, one may identify the DNA/cellular lesions required to switch on PCD.

Although we favor the hypothesis that the DNA damage in *tso2 rnr2a* triggers PCD, alternative mechanisms could not be excluded. For example, a reduction of dNTP may directly serve as a signal to trigger PCD. Perturbation of dNTP pools has been suggested to trigger DNA fragmentation and cell death in mammalian cells (Oliver et al., 1996). Another possible trigger for PCD may be the formation of defective chloroplasts or mitochondria in these *tso2 rnr2a* mutants. The malfunction of these organelles may lead to the release of reactive oxygen species or cytochrome *c*, which may subsequently trigger PCD in the *tso2 rnr2a* double mutants. Nevertheless, the leaves of *tso2 rnr2a* seedlings, which showed massive PCD, did not exhibit the white sectors that are hallmarks of *tso2-1* single mutants. A lack of correlation between white sectors in leaves and PCD suggests that chloroplast defects are unlikely to underlie PCD in *tso2 rnr2a*. Future experiments are necessary to further test hypotheses regarding the trigger for PCD in *tso2 rnr2a*. The availability of single and double mutations in all three *R2* genes provides a unique opportunity to identify suppressor mutations in genes that act upstream and downstream of RNR, providing insights into DNA damage checkpoint pathways and DNA damage–induced PCD in higher plants.

METHODS

Plant Growth, Mutant Strains, and Materials

Arabidopsis thaliana plants were grown under a 16-h-light/8-h-dark cycle at 20°C. *tso2-1*, *-2*, *-3*, and *-4* alleles were isolated in two separate EMS mutagenesis screens (Liu and Meyerowitz, 1995; Levin et al., 1998), and all four alleles were generated in the L*er* background. *rnr2a-1* was identified by the TILLING facility (McCallum et al., 2000). Specifically, the primer pair 5′-TTTGCTGTGAGGCTGGTCGCTTTT-3′ and 5′-CTTCC-AGATTCGATGGCGGATTCA-3′ was used to amplify ~1 kb of *RNR2A* genomic DNA from EMS-mutagenized Col-*er* M2 plants. HPLC-based detection of DNA heteroduplex led to the identification of *rnr2a-1*. Finally, primer pair 5′-CGATTAAATCTTCTTCACCGGA-3′ and 5′-GGCTCCAA-TCCTTTTTGGAT-3′ was used to PCR-amplify the entire *RNR2B* genomic DNA from three different *Arabidopsis* accessions: Col, L*er*, and Ws. Sequence analyses revealed 14 differences between Col and L*er*/Ws (Figure 2C). *TSO2* was provided by the Kazusa DNA Research Institute.

Microscopy

For scanning electron microscopy, inflorescences were fixed, coated, dissected, and photographed as described previously (Bowman et al., 1989). Images were directly captured with the semicaps software and the AMRAY 1000A scanning electron microscope. Whole-mount floral photomicrographs were taken through a Zeiss Stemi SV6 dissecting microscope. Slides containing longitudinal sections of inflorescence from in situ hybridization experiments were examined and photographed with a Nikon ECL1PSE E600W microscope with Nomarski optics equipped with a DXM1200 digital still camera. Images from the comet assay and the aniline blue staining were captured with the Nikon Labophot-2 microscope equipped with fluorescein isothiocyanate and UV light filters using ×20 objectives and a Nikon digital camera.

Map-Based Cloning of *TSO2*

tso2-1 (L*er*) was crossed to *sup-2* (Col). A total of 358 F2 *tso2-1* plants were assayed individually for linkage to various CAPS and dCAPS markers (see Supplemental Table 1 online), which mapped *TSO2* to a 20-kb region within the P1 clone MOJ10. A cosmid library was constructed from MOJ10 using binary vector pCLD04541. Two overlapped cosmids, D and G, were transformed into *tso2-1* mutants, and all eight transgenic plants harboring cosmid D but none of the five transgenic plants harboring cosmid G were wild type in phenotype, suggesting that cosmid D, not G, contains the *TSO2* gene. Sequencing of the four candidate genes *At3g27040*, *At3g27050*, *At3g27060*, and *At3g27070* in cosmid D identified only a mutation in *At3g27060* in *tso2-1*.

Molecular Analyses of *TSO2*, *RNR2A*, and *RNR2B*

p35S:*RNR2B-L* was constructed by PCR-amplifying the open reading frame using L*er* genomic DNA as a template and primer pair 5′-GCTCTAGACGATTAAATCTTCTTCACCGGA-3′ and 5′-CGGGATCCGGCTCCAATCCTTTTTGGAT-3′. The PCR fragment was inserted into the pBI121 vector (Clontech) using *Xba*I and *Bam*HI. To construct *p35S*:*RNR2A*, mRNA isolated from wild-type (Col) inflorescences was reversed-transcribed into cDNA with oligo(dT) primer and SuperScript reverse transcriptase (Invitrogen). The first-strand cDNA served as the template for PCR with Expand high-fidelity DNA polymerase (Roche) using primer pair 5′-GCTCTAGAGAATTCGAGATAATGGGTTCG-3′ and 5′-CGGGATCCCAATGGAGAAGGGACAAGTGA-3′. The PCR products of *RNR2A* cDNA were digested with *Xba*I and *Bam*HI and inserted into the pBI121 vector. The *pBI121-RNR2A* clones were sequenced to verify that the clones contained no mutation.

For *pTSO2*:*GUS* reporter constructs, a 2.1-kb *Bam*HI/*Eco*RI fragment containing the GUS open reading frame and 3′ Nos was excised from pBI121 and inserted into the *Bam*HI/*Eco*RI site of pBIN20 (Hennegan and Danna, 1998) to create the pBIN20GUS vector. A 1.2-kb promoter sequence of *TSO2* was PCR-amplified with primer pair 5′-GCTCTAGAA-TAAGGCCCTGTTCGTTTCC-3′ and 5′-CGGGATCCGAATCTGTCTGG-GGTTGGTG-3′. PCR products were digested with *Bam*HI/*Xba*I and inserted into *Bam*HI/*Xba*I-digested pBIN20GUS vector. All PCRs were performed with high-fidelity DNA polymerase Pwo or Tgo (Roche).

For semiquantitative RT-PCR, total RNA was isolated with Tri-Reagent (Sigma-Aldrich) from the wild type (L*er*), including 1-week-old roots and seedlings, 2-week-old rosette leaves, and 4-week-old cauline leaves, stems, and inflorescences. Two micrograms of total RNA was used to synthesize cDNA with oligo(dT) and SuperScript II reverse transcriptase (Invitrogen). PCR was conducted with 1 μL of diluted RT reaction at 94°C for 20 s, 57°C for 20 s, and 72°C for 40 s for 20 to 25 cycles. The PCR products were DNA gel-blotted and hybridized with a *RNR2B*-specific probe PCR amplified using primers 5′-CAAGCTTGACGAGGATTTTT-3′ and 5′-GTGCTCCCTCTGCCAATAAA-3′. To assay the induction of cell death– and DNA damage–induced markers and the induction of *TSI*, RNA was isolated from 3-week-old seedlings using protocols and conditions similar to those described above. Primer sequences for all RT-PCRs are listed in Supplemental Table 2 online.

In situ hybridization was essentially as described previously (Liu et al., 2000) except that the RNA probes were synthesized using the DIG RNA labeling kit (SP6/T7) (Roche) and were not hydrolyzed. The *TSO2* EST clone (RZL13g10F) was linearized with *Hin*dIII and served as a template for the *TSO2* antisense probe using the T7 promoter. For the in situ hybridization shown in Figure 5, a cDNA clone of *CycB1* (*pCYC1At*) (Hemerly et al., 1992) was obtained from Dirk Inze. *pCYC1At* was linearized with *Cla*I and served as the template for transcription to generate antisense and sense *CycB1* RNA probes from T7 and SP6 promoters, respectively. A *H4* EST clone (249N16) served as the template for PCR with primer pair 5′-TGGAAAGGGAGGAAAAGGTT-3′ and 5′-AACCCAGAAAACACAAACGC-3′. The 339-bp PCR product was cloned into the pCRII-TOPO vector (Invitrogen). Two clones containing inserts in opposite orientations relative to the T7 promoter were linearized with *Hin*dIII and served as templates for in vitro transcription from the T7 promoter to generate antisense and sense *H4* RNA probes.

Genetic Analyses

tso2-1 (L*er*) was crossed with *rnr2a-1 rnr2b-1* (Col). The F1 progeny heterozygous for all three mutations are wild type. dCAPS and CAPS markers (see Supplemental Table 1 online) were used to screen *tso2*-like F2 plants at *RNR2A* and *RNR2B* loci to identify the plants of various genotypes shown in Figure 3H. PCR-based genotyping was performed for individual seeds from *tso2-1*/*tso2-1; rnr2b-1*/+ parents. *tso2-1 rnr2b-1* double mutants were detected only among aborted seeds (Table 1). Finally, the *rnr2a-1*/*rnr2a-1; tso2-1*/+ plants, which are phenotypically normal, were identified from the same cross described above by PCR-based genotyping of normal-looking plants in F2. *tso2-1 rnr2a-1* double mutants were obtained from the self progeny of a *rnr2a-1*/*rnr2a-1; tso2-1*/+ parent.

Drug Treatment of *pTSO2*:*GUS* Transgenic Plants

Seeds of *pTSO2*:*GUS* transgenic T2 plants of L*er* ecotype were germinated on wet filter paper. One- to 2-d-old seedlings were then transferred to a 24-well plate containing 1 mL of water (nontreatment control), 0.5% colchicine, or 5 μg/mL aphidicolin. After 26 h, the seedlings were rinsed twice with water, stained overnight with 5-bromo-4-chloro-3-indolyl-β-glucuronic acid based on a previously described protocol (Parcy et al., 1998), and then photographed. Five different *pTSO2*:*GUS* transgenic lines and 15 to 20

T2 seedlings of each transgenic line were analyzed. Three T2 lines exhibited the same reported responses to different drug treatments.

Measuring dNTP Levels

The dNTP pool was measured by a polymerase-based assay (Roy et al., 1999). Inflorescences with unopened flower buds were harvested in liquid nitrogen, ground to a fine powder, weighed, and extracted with 60% cold methanol by vigorous vortexing. The extracts were heated at 95°C for 5 min and centrifuged at 17,000*g* for 15 min. The supernatants were dried in a Speedvac, resuspended in sterile distilled water, and stored at −20°C. One microliter of each sample was used for the polymerase assay. Commercial dNTPs were tested in parallel to establish a linear calibration curve. As the internal control, a portion of the ground tissues was assayed for alcohol dehydrogenase activity (Russell et al., 1990). The alcohol dehydrogenase activity per gram of sample was then used to normalize the dNTP level for each gram of ground tissues.

Comet Assay for DNA Damage

The CometAssay kit from Trevigen (Gaithersburg, MD) was used with minor modifications. Seedlings were chopped with a razor in a Petri dish kept on ice and containing 500 μL of 1× PBS plus 20 mM EDTA. The resulting mixture was filtered through a 60-μm nylon mesh. Forty microliters of nuclei was mixed with 400 μL of 1% low-melting-point agarose (prewarmed at 37°C) and placed onto Trevigen-precoated slides. After incubating in lysis solution (2.5 M NaCl, 100 mM EDTA, pH 10, 10 mM Tris, 1% sodium lauryl sarcosinate, and 1% Triton X-100) for 1 h at 4°C, the nuclei on slides were unwound in alkaline solution (0.3 N NaOH and 5 mM EDTA) for 40 min and neutralized two to three times in 1× TBE (Tris-borate/EDTA) for 5 min. The slides were run at 1 V/cm for 10 min in 1× TBE and then dipped in 70% ethanol for 5 min. After air-drying, the slides were stained with a 1:10,000 dilution of SYBR green. Antifade solution (1% *p*-phenylenediamine dihydrochloride in 0.1× PBS and 90% glycerol) was added to slides that were examined by epifluorescence microscopy. The percentage of DNA in each comet tail (T DNA%) was evaluated with the Comet Score software (http://www.autocomet.com) and assigned a number (0 to 4), with a higher number corresponding to a higher T DNA% (Collins et al., 1997). DNA damage units for each genotype were derived by averaging the data from four slides. One hundred comets were scored per slide.

UV-C Light Treatment

Ten-day-old seedlings were irradiated at various doses of UV-C light using Stratalinker 1800 (Stratagene). Because the UV light detector of Stratalinker is situated 15 cm from the UV lamps, the UV-C light dosage presented in Figure 7A was calculated to reflect the 5-cm distance from seedlings to the UV lamps based on the formula that the UV-C dosage is a function of the square of the distance. After UV-C irradiation, seedlings were grown under F40GO gold fluorescent lights for 5 d to avoid photoreactivation. Plants were returned to normal lighting for 1 to 2 weeks before survival rate was scored. To test *tso2-1 rnr2a-1*, a large number of F2 seeds of *tso2-1*/+*; rnr2a-1/rnr2a-1* were planted. One week after germination, *tso2-1 rnr2a-1* double mutant seedlings were easily distinguished from siblings of *tso2-1*/+*; rnr2a-1/rnr2a-1* or +/+*; rnr2a-1/rnr2a-1* genotype. These siblings were pulled from the soil. Approximately 30 *tso2-1 rnr2a-1* seedlings were left in each pot for UV-C light treatment.

Cell Death Assays

For trypan blue assay (Rate et al., 1999), 10-d-old rosette leaves were boiled in lactophenol containing 10 mg of trypan blue for 1 min, cleared in alcoholic lactophenol (95% ethanol:lactophenol, 2:1) for 2 min, washed in 50% ethanol, and stored in water. For aniline blue staining of callose (Rate et al., 1999), 10-d-old rosette leaves were boiled for 2 min in alcoholic lactophenol, rinsed in 50% ethanol, and then rinsed in water. Cleared and rinsed leaves were stained for 1 h at room temperature in a solution of 0.05% aniline blue in 0.15 M K_2HPO_4. Stained leaves were examined under UV epifluorescence. The 3,3′-diaminobenzidine uptake method (Thordal-Christensen et al., 1997) was used to detect H_2O_2. Ten-day-old seedlings were placed in 1 mg/mL 3,3′-diaminobenzidine in 10 mM ascorbic acid for 2 h. The seedlings were then boiled in 96% ethanol for 10 min and stored in 96% ethanol. H_2O_2 production is visualized as reddish-brown coloration.

The TUNEL assay was performed using the In Situ Cell Death Detection Kit-Fluorescein (Roche Diagnostics). Before detection, wild-type (L*er*) and *tso2-1 rnr2a-1* seedlings were fixed in 4% paraformaldehyde in 1× PBS at 4°C overnight and embedded in paraplasts. Eight-micrometer sections on glass slides were dewaxed in xylene, rehydrated, and then pretreated with 20 μg/mL proteinase K in 10 mM Tris-Cl, pH 7.5, for 20 min at room temperature. Two slides, treated with 1500 units/mL DNase I in 50 mM Tris-Cl, pH 7.5, 1 mM $MgSO_4$, and 1 mg/mL BSA for 20 min at room temperature, served as positive controls. Two slides, labeled in the absence of the terminal deoxyribonucleotidyl transferase enzyme, served as negative controls. Vectashield mounting medium (Vector Laboratories) and DAPI (1 μg/mL) were used to mount the slides before they were viewed and photographed with a Zeiss Axiophot microscope.

Accession Numbers

The *RNR2B* sequence from L*er* was submitted to GenBank with the accession number AY178109. The locus identifier numbers for *TSO2*, *RNR2A*, and *RNR2B* are At3g27060, At3g23580, and At5g40942, respectively. The accession number for *TSO2* cDNA is RZL13g10F (AV546418).

Supplemental Data

The following materials are available in the online version of this article.

Supplemental Table 1. PCR-Based Molecular Markers Developed for This Study.

Supplemental Table 2. Primer Sequences Used in Semiquantitative RT-PCR.

ACKNOWLEDGMENTS

We thank the ABRC and the Kazusa DNA Research Institute for DNA clones and seed stocks, Joshua Levin for *tso2* alleles, Dirk Inze for the *pCYC1At* clone, *Arabidopsis* TILLING for identifying *rnr2a-1*, and Roy Beatrice for advice and protocol in dNTP measurement. We thank Eric Baehrecke, Caren Chang, Robert Franks, Steve Mount, Shin Takeda, Lee Zou, and members of the Liu laboratory for comments on the manuscript. We thank Tim Mougel for microscopy assistance (contribution no. 97 of the Laboratory for Biological Ultrastructure, University of Maryland, College Park). This work was supported by U.S. Department of Energy Grant 02-00ER20281 to Z.L.

Received August 11, 2005; revised November 12, 2005; accepted November 30, 2005; published January 6, 2006.

REFERENCES

Angelis, K.J., Dusinska, M., and Collins, A.R. (1999). Single cell gel electrophoresis: Detection of DNA damage at different levels of sensitivity. Electrophoresis **20,** 2133–2138.

Bowman, J.L., Smyth, D.R., and Meyerowitz, E.M. (1989). Genes directing flower development in Arabidopsis. Plant Cell **1,** 37–52.

Brodersen, P., Petersen, M., Pike, H.M., Olszak, B., Skov, S., Odum, N., Jorgensen, L.B., Brown, R.E., and Mundy, J. (2002). Knockout of Arabidopsis accelerated-cell-death11 encoding a sphingosine transfer protein causes activation of programmed cell death and defense. Genes Dev. **16,** 490–502.

Bundock, P., and Hooykaas, P. (2002). Severe developmental defects, hypersensitivity to DNA-damaging agents, and lengthened telomeres in Arabidopsis MRE11 mutants. Plant Cell **14,** 2451–2462.

Chabes, A., Domkin, V., and Thelander, L. (1999). Yeast Sml1, a protein inhibitor of ribonucleotide reductase. J. Biol. Chem. **274,** 36679–36683.

Chabes, A., Georgieva, B., Domkin, V., Zhao, X., Rothstein, R., and Thelander, L. (2003a). Survival of DNA damage in yeast directly depends on increased dNTP levels allowed by relaxed feedback inhibition of ribonucleotide reductase. Cell **112,** 391–401.

Chabes, A., and Thelander, L. (2003). DNA building blocks at the foundation of better survival. Cell Cycle **2,** 171–173.

Chabes, A.L., Pfleger, C.M., Kirschner, M.W., and Thelander, L. (2003b). Mouse ribonucleotide reductase R2 protein: A new target for anaphase-promoting complex-Cdh1-mediated proteolysis. Proc. Natl. Acad. Sci. USA **100,** 3925–3929.

Chaboute, M.E., Clement, B., and Philipps, G. (2002). S phase and meristem-specific expression of the tobacco RNR1b gene is mediated by an E2F element located in the 5′ leader sequence. J. Biol. Chem. **277,** 17845–17851.

Chaboute, M.E., Clement, B., Sekine, M., Philipps, G., and Chaubet-Gigot, N. (2000). Cell cycle regulation of the tobacco ribonucleotide reductase small subunit gene is mediated by E2F-like elements. Plant Cell **12,** 1987–2000.

Chaboute, M.E., Combettes, B., Clement, B., Gigot, C., and Philipps, G. (1998). Molecular characterization of tobacco ribonucleotide reductase RNR1 and RNR2 cDNAs and cell cycle-regulated expression in synchronized plant cells. Plant Mol. Biol. **38,** 797–806.

Chen, I.P., Haehnel, U., Altschmied, L., Schubert, I., and Puchta, H. (2003). The transcriptional response of Arabidopsis to genotoxic stress—A high-density colony array study (HDCA). Plant J. **35,** 771–786.

Chernova, O.B., Chernov, M.V., Agarwal, M.L., Taylor, W.R., and Stark, G.R. (1995). The role of p53 in regulating genomic stability when DNA and RNA synthesis are inhibited. Trends Biochem. Sci. **20,** 431–434.

Collins, A., Dusinska, M., Franklin, M., Somorovska, M., Petrovska, H., Duthie, S., Fillion, L., Panayiotidis, M., Raslova, K., and Vaughan, N. (1997). Comet assay in human biomonitoring studies: Reliability, validation, and applications. Environ. Mol. Mutagen. **30,** 139–146.

Culligan, K., Tissier, A., and Britt, A. (2004). ATR regulates a G2-phase cell-cycle checkpoint in *Arabidopsis thaliana.* Plant Cell **16,** 1091–1104.

Danon, A., and Gallois, P. (1998). UV-C radiation induces apoptotic-like changes in *Arabidopsis thaliana.* FEBS Lett. **437,** 131–136.

Danon, A., Rotari, V.I., Gordon, A., Mailhac, N., and Gallois, P. (2004). Ultraviolet-C overexposure induces programmed cell death in Arabidopsis, which is mediated by caspase-like activities and which can be suppressed by caspase inhibitors, p35 and Defender against Apoptotic Death. J. Biol. Chem. **279,** 779–787.

Dietrich, R.A., Delaney, T.P., Uknes, S.J., Ward, E.R., Ryals, J.A., and Dangl, J.L. (1994). Arabidopsis mutants simulating disease resistance response. Cell **77,** 565–577.

Doucet-Chabeaud, G., Godon, C., Brutesco, C., de Murcia, G., and Kazmaier, M. (2001). Ionising radiation induces the expression of PARP-1 and PARP-2 genes in Arabidopsis. Mol. Genet. Genomics **265,** 954–963.

Doutriaux, M.P., Couteau, F., Bergounioux, C., and White, C. (1998). Isolation and characterisation of the RAD51 and DMC1 homologs from *Arabidopsis thaliana.* Mol. Gen. Genet. **257,** 283–291.

Downes, C.S., Bachrati, C.Z., Devlin, S.J., Tommasino, M., Cutts, T.J., Watson, J.V., Rasko, I., and Johnson, R.T. (2000). Mammalian S-phase checkpoint integrity is dependent on transformation status and purine deoxyribonucleosides. J. Cell Sci. **113,** 1089–1096.

Elledge, S.J., Zhou, Z., and Allen, J.B. (1992). Ribonucleotide reductase: Regulation, regulation, regulation. Trends Biochem. Sci. **17,** 119–123.

Fobert, P.R., Coen, E.S., Murphy, G.J., and Doonan, J.H. (1994). Patterns of cell division revealed by transcriptional regulation of genes during the cell cycle in plants. EMBO J. **13,** 616–624.

Greenberg, J.T. (1996). Programmed cell death: A way of life for plants. Proc. Natl. Acad. Sci. USA **93,** 12094–12097.

Greenberg, J.T., and Yao, N. (2004). The role and regulation of programmed cell death in plant-pathogen interactions. Cell. Microbiol. **6,** 201–211.

Hartung, F., Angelis, K.J., Meister, A., Schubert, I., Melzer, M., and Puchta, H. (2002). An archaebacterial topoisomerase homolog not present in other eukaryotes is indispensable for cell proliferation of plants. Curr. Biol. **12,** 1787–1791.

Hemerly, A., Bergounioux, C., Van Montagu, M., Inze, D., and Ferreira, P. (1992). Genes regulating the plant cell cycle: Isolation of a mitotic-like cyclin from *Arabidopsis thaliana.* Proc. Natl. Acad. Sci. USA **89,** 3295–3299.

Hennegan, K.P., and Danna, K.J. (1998). pBIN20: an improved binary vector for *Agrobacterium*-mediated transformation. Plant Mol. Biol. Rep. **16,** 129–131.

Huang, M., Zhou, Z., and Elledge, S.J. (1998). The DNA replication and damage checkpoint pathways induce transcription by inhibition of the Crt1 repressor. Cell **94,** 595–605.

Kaya, H., Shibahara, K.I., Taoka, K.I., Iwabuchi, M., Stillman, B., and Araki, T. (2001). FASCIATA genes for chromatin assembly factor-1 in Arabidopsis maintain the cellular organization of apical meristems. Cell **104,** 131–142.

Kimura, T., Takeda, S., Sagiya, Y., Gotoh, M., Nakamura, Y., and Arakawa, H. (2003). Impaired function of p53R2 in Rrm2b-null mice causes severe renal failure through attenuation of dNTP pools. Nat. Genet. **34,** 440–445.

Kolberg, M., Strand, K.R., Graff, P., and Andersson, K.K. (2004). Structure, function, and mechanism of ribonucleotide reductases. Biochim. Biophys. Acta **1699,** 1–34.

Kressel, M., and Groscurth, P. (1994). Distinction of apoptotic and necrotic cell death by in situ labelling of fragmented DNA. Cell Tissue Res. **278,** 549–556.

Kuriyama, H., and Fukuda, H. (2002). Developmental programmed cell death in plants. Curr. Opin. Plant Biol. **5,** 568–573.

Levin, J.Z., Fletcher, J.C., Chen, X., and Meyerowitz, E.M. (1998). A genetic screen for modifiers of UFO meristem activity identifies three novel FUSED FLORAL ORGANS genes required for early flower development in Arabidopsis. Genetics **149,** 579–595.

Lincker, F., Philipps, G., and Chaboute, M.E. (2004). UV-C response of the ribonucleotide reductase large subunit involves both E2F-mediated gene transcriptional regulation and protein subcellular relocalization in tobacco cells. Nucleic Acids Res. **32,** 1430–1438.

Liu, C., Powell, K.A., Mundt, K., Wu, L., Carr, A.M., and Caspari, T. (2003). Cop9/signalosome subunits and Pcu4 regulate ribonucleotide reductase by both checkpoint-dependent and -independent mechanisms. Genes Dev. **17,** 1130–1140.

Liu, Z., Franks, R.G., and Klink, V.P. (2000). Regulation of gynoecium marginal tissue formation by LEUNIG and AINTEGUMENTA. Plant Cell **12,** 1879–1892.

Liu, Z., and Meyerowitz, E.M. (1995). LEUNIG regulates AGAMOUS expression in Arabidopsis flowers. Development **121,** 975–991.

Liu, Z., Running, M.P., and Meyerowitz, E.M. (1997). TSO1 functions in cell division during Arabidopsis flower development. Development **124,** 665–672.

Mayer, K.F., Schoof, H., Haecker, A., Lenhard, M., Jurgens, G., and Laux, T. (1998). Role of WUSCHEL in regulating stem cell fate in the Arabidopsis shoot meristem. Cell **95,** 805–815.

McCallum, C.M., Comai, L., Greene, E.A., and Henikoff, S. (2000). Targeting induced local lesions in genomes (TILLING) for plant functional genomics. Plant Physiol. **123,** 439–442.

Miller, J.D., Arteca, R.N., and Pell, E.J. (1999). Senescence-associated gene expression during ozone-induced leaf senescence in Arabidopsis. Plant Physiol. **120,** 1015–1024.

Oliver, F.J., Collins, M.K., and Lopez-Rivas, A. (1996). dNTP pools imbalance as a signal to initiate apoptosis. Experientia **52,** 995–1000.

Osakabe, K., Yoshioka, T., Ichikawa, H., and Toki, S. (2002). Molecular cloning and characterization of RAD51-like genes from *Arabidopsis thaliana.* Plant Mol. Biol. **50,** 71–81.

Parcy, F., Nilsson, O., Busch, M.A., Lee, I., and Weigel, D. (1998). A genetic framework for floral patterning. Nature **395,** 561–566.

Philipps, G., Clement, B., and Gigot, C. (1995). Molecular characterization and cell cycle-regulated expression of a cDNA clone from *Arabidopsis thaliana* homologous to the small subunit of ribonucleotide reductase. FEBS Lett. **358,** 67–70.

Pontier, D., Gan, S., Amasino, R.M., Roby, D., and Lam, E. (1999). Markers for hypersensitive response and senescence show distinct patterns of expression. Plant Mol. Biol. **39,** 1243–1255.

Rate, D.N., Cuenca, J.V., Bowman, G.R., Guttman, D.S., and Greenberg, J.T. (1999). The gain-of-function Arabidopsis acd6 mutant reveals novel regulation and function of the salicylic acid signaling pathway in controlling cell death, defenses, and cell growth. Plant Cell **11,** 1695–1708.

Reichard, P. (1988). Interactions between deoxyribonucleotide and DNA synthesis. Annu. Rev. Biochem. **57,** 349–374.

Riha, K., McKnight, T.D., Griffing, L.R., and Shippen, D.E. (2001). Living with genome instability: Plant responses to telomere dysfunction. Science **291,** 1797–1800.

Roy, B., Beuneu, C., Roux, P., Buc, H., Lemaire, G., and Lepoivre, M. (1999). Simultaneous determination of pyrimidine or purine deoxyribonucleoside triphosphates using a polymerase assay. Anal. Biochem. **269,** 403–409.

Russell, D.A., Wong, D.M.L., and Sachs, M.M. (1990). The anaerobic response of soybean. Plant Physiol. **92,** 401–407.

Saada, A., Shaag, A., Mandel, H., Nevo, Y., Eriksson, S., and Elpeleg, O. (2001). Mutant mitochondrial thymidine kinase in mitochondrial DNA depletion myopathy. Nat. Genet. **29,** 342–344.

Saitoh, S., Chabes, A., McDonald, W.H., Thelander, L., Yates, J.R., and Russell, P. (2002). Cid13 is a cytoplasmic poly(A) polymerase that regulates ribonucleotide reductase mRNA. Cell **109,** 563–573.

Schmid, M., Davison, T.S., Henz, S.R., Pape, U.J., Demar, M., Vingron, M., Scholkopf, B., Weigel, D., and Lohmann, J.U. (2005). A gene expression map of *Arabidopsis thaliana* development. Nat. Genet. **37,** 501–506.

Siddiqui, N.U., Stronghill, P.E., Dengler, R.E., Hasenkampf, C.A., and Riggs, C.D. (2003). Mutations in Arabidopsis condensin genes disrupt embryogenesis, meristem organization and segregation of homologous chromosomes during meiosis. Development **130,** 3283–3295.

Steimer, A., Amedeo, P., Afsar, K., Fransz, P., Scheid, O.M., and Paszkowski, J. (2000). Endogenous targets of transcriptional gene silencing in Arabidopsis. Plant Cell **12,** 1165–1178.

Takeda, S., Tadele, Z., Hofmann, I., Probst, A.V., Angelis, K.J., Kaya, H., Araki, T., Mengiste, T., Scheid, O.M., Shibahara, K., Scheel, D., and Paszkowski, J. (2004). BRU1, a novel link between responses to DNA damage and epigenetic gene silencing in Arabidopsis. Genes Dev. **18,** 782–793.

Tanaka, H., Arakawa, H., Yamaguchi, T., Shiraishi, K., Fukuda, S., Matsui, K., Takei, Y., and Nakamura, Y. (2000). A ribonucleotide reductase gene involved in a p53-dependent cell-cycle checkpoint for DNA damage. Nature **404,** 42–49.

Thordal-Christensen, H., Zhang, Z., Wei, Y., and Collinge, D.B. (1997). Subcellular localization of H_2O_2 in plants: H_2O_2 accumulation in papillae and hypersensitive response during the barley-powdery mildew interaction. Plant J. **11,** 1187–1194.

Vogelstein, B., Lane, D., and Levine, A.J. (2000). Surfing the p53 network. Nature **408,** 307–310.

West, C.E., Waterworth, W.M., Story, G.W., Sunderland, P.A., Jiang, Q., and Bray, C.M. (2002). Disruption of the Arabidopsis AtKu80 gene demonstrates an essential role for AtKu80 protein in efficient repair of DNA double-strand breaks in vivo. Plant J. **31,** 517–528.

Whittle, C.A., Beardmore, T., and Johnston, M.O. (2001). Is G1 arrest in plant seeds induced by a p53-related pathway? Trends Plant Sci. **6,** 248–251.

Yao, R., Zhang, Z., An, X., Bucci, B., Perlstein, D.L., Stubbe, J., and Huang, M. (2003). Subcellular localization of yeast ribonucleotide reductase regulated by the DNA replication and damage checkpoint pathways. Proc. Natl. Acad. Sci. USA **100,** 6628–6633.

Zhao, X., Chabes, A., Domkin, V., Thelander, L., and Rothstein, R. (2001). The ribonucleotide reductase inhibitor Sml1 is a new target of the Mec1/Rad53 kinase cascade during growth and in response to DNA damage. EMBO J. **20,** 3544–3553.

Zhao, X., Georgieva, B., Chabes, A., Domkin, V., Ippel, J.H., Schleucher, J., Wijmenga, S., Thelander, L., and Rothstein, R. (2000). Mutational and structural analyses of the ribonucleotide reductase inhibitor Sml1 define its Rnr1 interaction domain whose inactivation allows suppression of mec1 and rad53 lethality. Mol. Cell. Biol. **20,** 9076–9083.

Zhao, X., Muller, E.G., and Rothstein, R. (1998). A suppressor of two essential checkpoint genes identifies a novel protein that negatively affects dNTP pools. Mol. Cell **2,** 329–340.